A-site Nonstoichiometric $Ba_xCo_{0.4}Fe_{0.4}Zr_{0.1}Y_{0.1}O_{3-\delta}$ Cathode for Protonic Ceramics Fuel Cells

Kangwei Wei[a,b,*], Zhiguo Guo[a,b], Fanglin Chen[c], Hong Liu[d], Yihan Ling[e,*]

a. School of Emergency Management and Safety Engineering, Jiangxi University of Science and Technology, Ganzhou 341000, P.R. China

b. Ganzhou Innovation Center for Comprehensive Emergency Technology of Multi-disasters, Jiangxi University of Science and Technology, Ganzhou, 341000, P.R. China

c. Department of Mechanical Engineering, University of South Carolina, Columbia, SC 29205, USA

d. School of Safety and Engineering, China University of Mining and Technology, Xuzhou 221116, P.R. China

e. School of Materials Science and Physics, China University of Mining and Technology, Xuzhou 221116, P.R. China

[*] Corresponding Author:

Yihan Ling* and Kangwei Wei*

School of Emergency Management and Safety Engineering,

Jiangxi University of Science and Technology, Ganzhou 341000, P.R. China

E-mail address: 1026807262@qq.com

ABSTRACT

Highly active triple (proton-, oxygen-ion-, and electron) conducting materials $Ba_xCo_{0.4}Fe_{0.4}Zr_{0.1}Y_{0.1}O_{3-\delta}$ (BxCFZY, x=0.9-1.1) were optimized as potential cathodes for protonic ceramics fuel cells (PCFCs) in this study. The crystal structure, oxygen vacancy concentration, electronic conductivity, oxygen transfer properties and electrochemical performance of BxCFZY oxides were systematically evaluated. The conductivity of BxCFZY decreases but oxygen vacancies increase with increasing Ba content, indicating that the charge compensation was mainly achieved by the production of oxygen vacancy rather than the increase in the valence of transition metal cations. The power density of 1170 mW cm^{-2} and the polarization resistance of 0.05 Ω cm^2 were achieved at 700°C for the anode supported cell with B1.1CFZY cathode, suggesting that the A-site excess on the BxCFZY had a positive effect on the catalytic activity for the oxygen reduction reaction. Furthermore, the distribution function of relaxation time (DRT) analysis method was adopted to determine the electrochemical processes of the cells with BxCFZY cathodes. The calculated results confirmed that the cell with B1.1CFZY cathode exhibited the optimum performance due to the best oxygen transfer properties in BxCFZY cathodes.

KEYWORDS: *protonic ceramics fuel cells,* $Ba_xCo_{0.4}Fe_{0.4}Zr_{0.1}Y_{0.1}O_{3-\delta}$*, charge compensation, DRT, oxygen transfer properties*

1. INTRODUCTION

The growing demand of fossil fuels has brought a great number of environmental problems and caused enormous strains on the energy supply. Hydrogen with the clean, storable and transportable characteristics has been identified as a promising secondary energy carrier. Among hydrogen conversion devices, solid oxide fuel cells (SOFCs) with low-emission, quietness and efficiency have received a broad audience.[1-3] However, for traditional oxide ionic SOFCs, the high operation temperature (800-1000°C) resulted in a series of problems such as the cell sealing, life and start-up time, severely hindering the commercialization of SOFCs.[4,5] The protonic ceramics fuel cells (PCFCs) with a favourite activation energy (Ea) of the H^+ transport can operate at a much lower temperature.[6-9] However, a challenge for PCFCs is the polarization losses of cathode which will greatly increase with the decrease in operating temperature.[10-12] Therefore, developing highly active cathode materials is essential to promote the oxygen reduction reaction (ORR) of PCFCs at reduced operating temperatures.

Among different oxide materials, the mixed ionic-electronic conductor (MIEC) ABO_3 is widely used as cathodes for PCFCs. In MIECs, $BaCoO_{3-\delta}$-based perovskite oxides with high conductivity and high electrocatalytic activity for ORR are extensively studied. The excellent conductivity comes from the small charge transfer gap and good bond strength between the Co and O.[13,14] Besides, large Ba ions can lead to the large free volume and thus reduce the migration Ea of oxygen ions in the lattice.[15] However, there is a problem for pure $BaCoO_3$ that the phase structure is easy to transform from cubic to hexagonal with decreasing the temperature. Two main

strategies are introduced to improve the phase stability: the deficiency or partial substitution of A or B site, such as $Ba_{0.9}Co_{0.7}Fe_{0.2}Nb_{0.1}O_{3-\delta}$[16], $Ba_{1-x}Sr_xCo_{0.8}Fe_{0.2}O_{3-\delta}$[17,18] and $BaCo_{0.7}Fe_{0.2}Nb_{0.1}O_{3-\delta}$[19,20]. Duan et al.[21] reported a promising new cathode $BaCo_{0.4}Fe_{0.4}Zr_{0.1}Y_{0.1}O_{3-\delta}$ (BCFZY) with triple-conducting character, achieving the peak power density (PPD) of 455 mW cm^{-2} when using H_2 at 500°C. The $H^+/O^{2-}/e^-$ triple-conducting BCFZY perovskite cathode can enhance the protonic, ionic and electronic conduction, and so increasing the number of active sites for electrochemical reactions. However, the phase stability was not good for BCFZY at low temperature, which can be attributed to the mismatch of A- and B-site ion radii. Recently, similar materials to BCFZY have also been intensively studied[22-25].

A-site nonstoichiometry of $BaCoO_{3-\delta}$-based perovskite oxides usually exhibits a great impact on the stability, conductivity, oxygen vacancy and electrochemical performance.[26-28] A-site deficient B0.90CFZY and the cell performance based on the composite cathode have been studied in our previous work, and the cell PPD was enhanced from ~450 to ~540 mW cm^{-2} at 700°C after adding $BaZr_{0.1}Ce_{0.7}Y_{0.2}O_{3-\delta}$ into B0.90CFZY.[29] However, to the best of our knowledge, there is still a lack of investigation about the impact of A-site nonstoichiometry on the electrochemical performance of BxCFZY. Herein, to search for the optimal cathode composition, we systematically evaluated the performance of BxCFZY (x=0.9-1.1) cathodes in PCFCs for the first time. Among the BxCFZY cathodes, B1.1CFZY composition exhibited best catalytic activity for ORR and highest power density in single cells, suggesting that A-site excess on the BxCFZY cathodes has a positive effect on the electrochemical

performance. The fastest oxygen species involved reactions and diffusion rate were further confirmed in B1.1CFZY cathode by DRT analysis.

2. EXPERIMENTAL SECTION

2.1. Powder Preparation. BxCFZY powders with x=0.9-1.1 were synthesized via a combustion method by using the EDTA-citrate complexes. The precursor chemicals $Ba(CH_3COO)_2$, $Co(NO_3)_2{\cdot}6H_2O$, $Fe(NO_3)_3{\cdot}9H_2O$, $Zr(NO_3)_4{\cdot}3H_2O$ and $Y(NO_3)_3{\cdot}6H_2O$ were mixed in the solution of EDTA and citric acid. The molar ratio of total metal ions, EDTA and citric acid is 0.8:1:1. The PH value was adjusted to ~7 by adding $NH_3{\cdot}H_2O$ in the solution. The solution was subsequently stirred and heated until self-combustion to form a solid precursor. Finally, powders were calcinated at 1100°C for 3 h to obtain BxCFZY cathode materials. In addition, cathode powders were uniaxially pressed into bar samples and then sintered at 1250°C for 3 h to measure the electrical conductivity.

2.2. Cell Fabrication. The cells with a configuration of Ni-BZCY (NiO-$BaZr_{0.1}Ce_{0.7}Y_{0.2}O_{3-\delta}$, support)/Ni-BZCY(functional layer)/BZCY/BxCFZY were constructed for electrochemical measurement. NiO-BZCY with a weight ratio of 60:40 was added 30 wt% starch and then milled for 2 h to obtain anode support powders. Then the support layer, functional layer (Ni-BZCY mixture without starch) and electrolyte powders were co-pressed to form the half-cells. Cathode powders were added into the terpineol·ethyl cellulose solution with a weight ratio of 1:1.5 and then manually milled in an agate mortar and pestle to obtain the slurry. The slurry was coated on the electrolyte surface of the half-cells with the effective area of 0.2 cm^2. The anode-supported single cells can then be obtained after firing at 1000°C for 3 h. Single cells

were finally sealed on alumina ceramic tubes for electrochemical tests.

2.3. Characterization. The phase structures of BxCFZY (x=0.9-1.1) were identified using XRD (DX-2700B). The sample powders were investigated using HR-TEM equipped with EDX detector. XPS was adopted to analyze the valence states of B-site ions in BxCFZY (x=0.9-1.1). The conductivity testing was performed at 300-800°C using a Keithley 2000 multimeter through a four-probe DC method. The polarization curves and electrochemical impedance spectra (EIS) of single cells at 700-550°C were obtained using the Electrochemical Workstation (Zennium, Zahner, Germany). The cell microstructure and composition were also checked using SEM equipped with EDS.

3. RESULTS AND DISCUSSION

3.1. Phase Structure. A single perovskite phase shown in Figure 1 was formed for BxCFZY compositions with x=0.9-1.1. The XRD patterns of all samples showed a symmetrical cubic perovskite structure without the existence of secondary phase. It can be found in Figure 1b that the main diffraction peaks of the BxCFZY perovskite oxides with barium deficiency shift to higher 2θ values, indicating the shrinkage of the perovskite lattice.[30,31] However, no obvious shift occurs on the main diffraction peaks of barium excess. The Rietveld refinement on XRD patterns of BxCFZY perovskite oxides is shown in Figure S1. The cell parameters of BxCFZY perovskite oxides from x=0.9 to 1.1 have been confirmed to be 4.097 Å, 4.098 Å, 4.127 Å, 4.128 Å and 4.129 Å, respectively, which is consistent with the change of its main diffraction peak and the results of other cathode materials such as $Ba_{1-x}Co_{0.9-y}Fe_yNb_{0.1}O_{3-\delta}$[30], $Ba_{1-x}Co_{0.7}Fe_{0.2}Nb_{0.1}O_{3-\delta}$[32] and $Gd_{1+x}Ba_{1+x}Co_2O_{5+\delta}$[33]. In general, the barium deficiency could

cause the oxidation of B-site ions or formation of oxygen vacancy as charge compensation. The production of oxygen vacancy would cause the lattice expansion, while B-site ions oxidized to a higher state could lead to the lattice shrinkage.[34,35] Therefore, the results suggest that the A-site barium deficiency is more favorable to B-site oxidation, but the contributions of oxygen vacancy production and oxidation of B-site cation on barium excess are likely comparable.

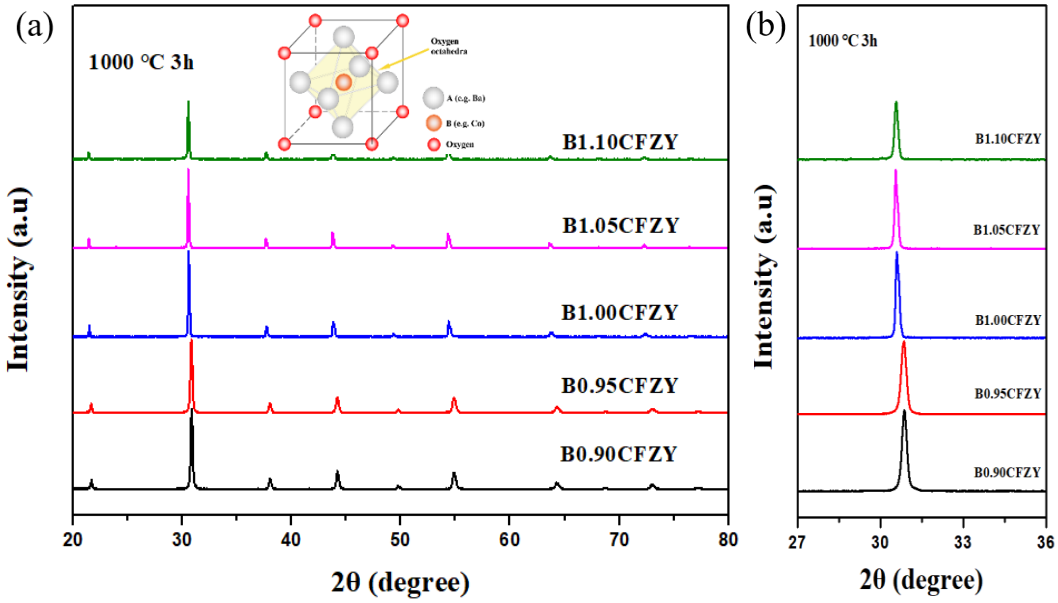

Figure 1. (a) XRD patterns of BxCFZY (x=0.9-1.1) calcined at 1000°C for 3h, (b) magnified in-situ XRD patterns from 27 to 36°C.

Crystal structures of BxCFZY samples were further characterized by HR-TEM. The reliability of all samples was also confirmed by EDX analysis (shown in Figure S2). Fourier transform was performed to determine the interplanar distances (d) of BxCFZY with x=0.9-1.1, as shown in Figure 2. The interplanar spacing of BxCFZY corresponding to (110) plane decreases from 3.32 Å to 2.94 Å as the value of x decreases from 1.1 to 0.95, which agrees with the results of XRD patterns. The lattice shrinkage caused the decrease of interplanar distance. Compared with B0.95CFZY sample, a slight expansion of interplanar distance was 2.96 Å on B0.9CFZY, which

could be explained that the excessive deficiency formed higher oxygen vacancy concentration and thus resulted in the lattice expansion.[15,29,32]

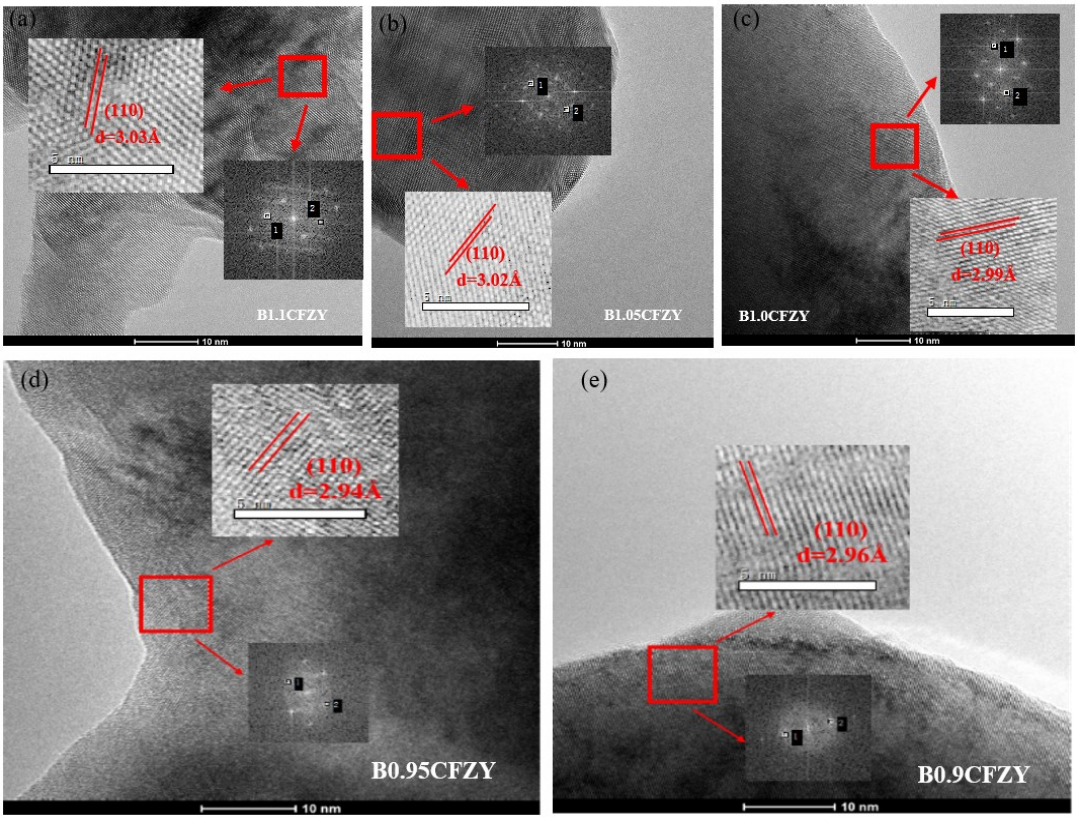

Figure 2. The high-resolution TEM images of BxCFZY with (a) x=1.1, (b) x=1.05, (c) x=1.0, (d) x=0.95, (e) x=0.9.

3.2. Electrical Conductivity. The electrical conductivity of the BxCFZY (x=0.9-1.1) as a function of temperature was obtained by using a four-probe DC method on sintered bar samples in air as shown in Figure 3. The conductivity of all samples increases gradually with increasing temperature, which showed the semi-conductivity behavior.[11,36] There is a slope change appearing at around 475°C, that is in good consistence with the previous work.[21] In general, increasing the temperature results in loss of lattice oxygen and formation of oxygen vacancy, leading to a decrease in the concentration of electronic holes as expressed by Eq. (1). [37,38] The slope change showing at around 475°C for all samples indicated that the electronic conductivity may

be the major dominating part above 475°C whereas ionic in the lower range of temperatures. [21, 39]

$$O_O^x + 2B_B^{\cdot} \rightarrow V_O^{\cdot\cdot} + 2B_B^{\times} + \frac{1}{2}O_2(g) \quad (1)$$

where "x" refers to neutrality with respect to the lattice, "•" represents unit positive charge with respect to the lattice, and V_0 refers to oxygen vacancies, $B^{\cdot}$ refers to tetravalent cations.

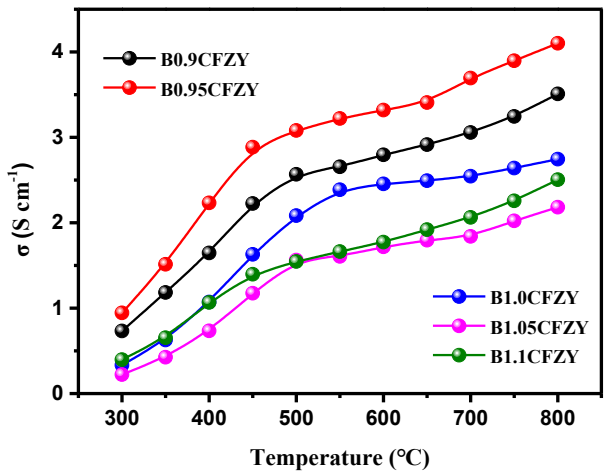

Figure 3. The conductivity of the BxCFZY (x = 0.9-1.1) samples in air as a function of temperature.

The conductivity is increasing when x decreases from 1.05 to 0.95, in agreement with the results of $Ba_{1-x}Co_{0.7}Fe_{0.2}Nb_{0.1}O_{3-\delta}$ [30]. The conductivity of 3.7 S cm^{-1} is achieved at 700°C for Ba0.95CFZY, which is much higher than the BZCY electrolyte with the conductivity of 0.025 S cm^{-1} at 700°C.[40] These results suggest that Ba deficiency in BxCFZY will boost B-site oxidation as evidenced from the shrinkage of the lattice parameters based on XRD results, while Ba excess in BxCFZY exhibited the low conductivity due to more oxygen vacancies formation. In addition, more Ba^{2+} with large ionic radius can also block electron migration and thus lead to the low conductivity. With the increase in Ba deficiency, the conductivity of Ba0.9CFZY was not further promoted, which can be ascribed to the excessive deficiency leading to the more oxygen

vacancies generation. The higher oxygen vacancy concentration will enhance the electrocatalytic activity for ORR due to the faster oxygen transfer and thus enhancement in the cell performance.

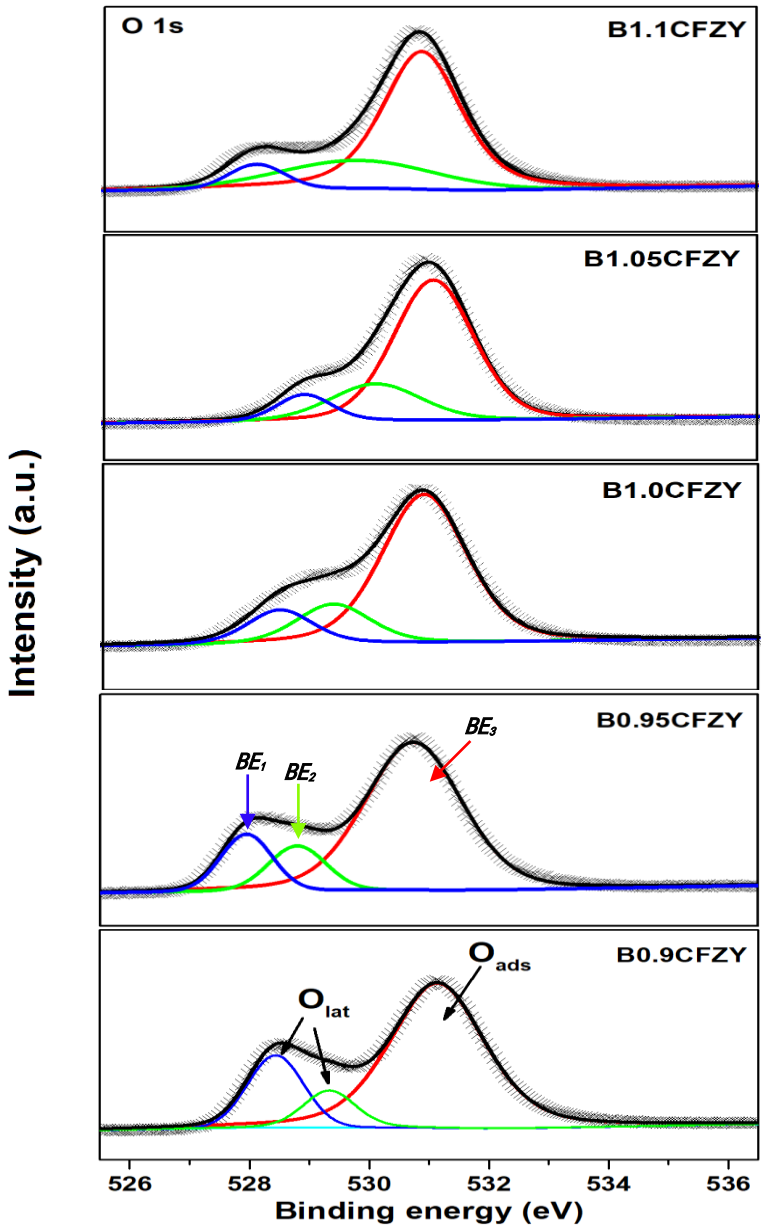

Figure 4. O1s core-level spectra of BxCFZY (x=0.9-1.1) at room temperature.

3.3. XPS Analysis. In general, the surface oxygen species have a significant effect on the rate-limiting step of ORR for the cathode. In order to investigate the different oxygen species existing on the BxCFZY surface, the O 1s core-level spectra of BxCFZY (x=0.9-1.1) were obtained by XPS analysis as shown in Figure 4. Three fitted

peaks BE_1, BE_2 and BE_3 exhibit in all the samples. The higher binding energy peak BE_3 locating at around 531 eV generally corresponds to the adsorbed oxygen (O_{ads}) such as the chemisorbed oxygen species (O^-, O^{2-} or O_2^{2-}).[41,42] The lower binding energy peaks BE_1 and BE_2 between 528 eV and 530 eV can be ascribed to the lattice oxygen (O_{lat}).[41] As the value of x decreases from 1.05 to 0.95, there is a clear shift of the peaks BE_1 and BE_2 toward lower binding energy, which is in accordance with the results of the lattice shrinkage. The area ratios of O_{abs}/O_{lat} were calculated and listed in Table 1. The O_{ads} concentration gradually increases and reaches the maximum value at x= 0.95, indicating that the Ba deficiency in BxCFZY materials is beneficial to the formation of the adsorbed oxygen.

3.4. The Chemical Stability of BxCFZY. At the cathode side, the existence of H_2O and CO_2 is a challenge to the stability of cathode materials in PCFCs. In order to investigate the H_2O and CO_2 tolerance of BxCFZY, the BxCFZY disks were treated in 100% concentration of CO_2 at 700°C for 10 h and boiling water for 5 h, respectively. Figure 5 shows the XRD results of BxCFZY samples treated in CO_2. No impurity phase was observed on all samples, confirming good chemical stability of BxCFZY in a high-CO_2 environment. However, a mixed O^{2-}/e^- conducting phase $BaCoO_{3-\delta}$ existed in B1.05CFZY and B1.10CFZY samples treated by H_2O. The $BaCoO_{3-\delta}$ phase can enhance the ionic and electronic conduction of the electrode, so that the interfaces between the three phases greatly increase the number of active sites for electrochemical reactions.[43]

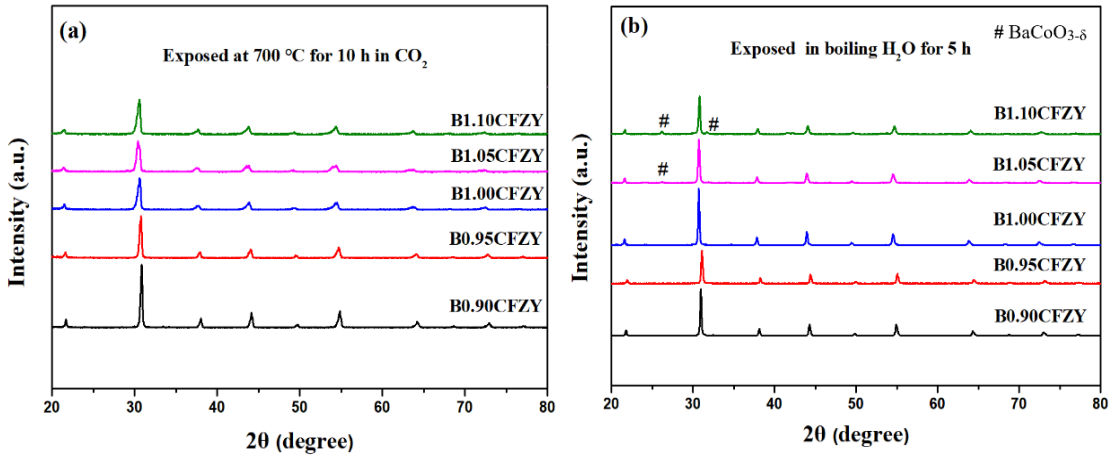

Figure 5. XRD spectra of BxCFZY treated by (a) CO_2 and (b) boiling H_2O.

3.5. Cell Performance. The performance of single cells with BxCFZY (x=0.9-1.1) cathodes operating under humidified H_2 (3% H_2O) was investigated. Figure 6a compared the electrochemical performance of BxCFZY at 700°C. It can be found that the peak power density was enhanced about 159 % from 452 to 1170 mW cm^{-2} when the A-site nonstoichiometry x increased from 0.9 to 1.1 In addition, the open-circuit voltage (OCV) also got an obvious promotion (0.96-1.02 V), probably because B1.1CFZY cathode had a better oxygen capture capability that resulted in a higher oxygen partial pressure at the cathode side, indicative of better electrocatalytic oxygen reduction activity for B1.1CFZY cathode. This may be ascribed to the excess of A-site barium leading to a higher oxygen vacancy concentration. Figure 6b shows the cell performance with B1.1CFZY cathode at 700-550°C. The OCV increases from 1.02 to 1.07 V when decreasing temperature form 700°C to 550°C. The corresponding PPD is 1170, 934, 597 and 365 mW cm^{-2}, respectively, higher performance compared to other PCFCs using $BaCoO_{3-\delta}$-based perovskite oxides as cathodes[44-46] and the YSZ-based SOFCs using BCFZY or $BaCo_{0.4}Fe_{0.4}Zr_{0.1}Y_{0.1}O_{2.95-\delta}F_{0.05}$ as cathode[47], even though B1.1CFZY exhibited a lower electronic conductivity in BxCFZY materials. The

excellent electrochemical performance confirms the sufficient oxygen reduction activity when using B1.1CFZY as cathode in PCFCs. The results suggest that higher oxygen vacancy concentration of A-site excessive BxCFZY has a dominant effect on the catalytic activity of cathode.

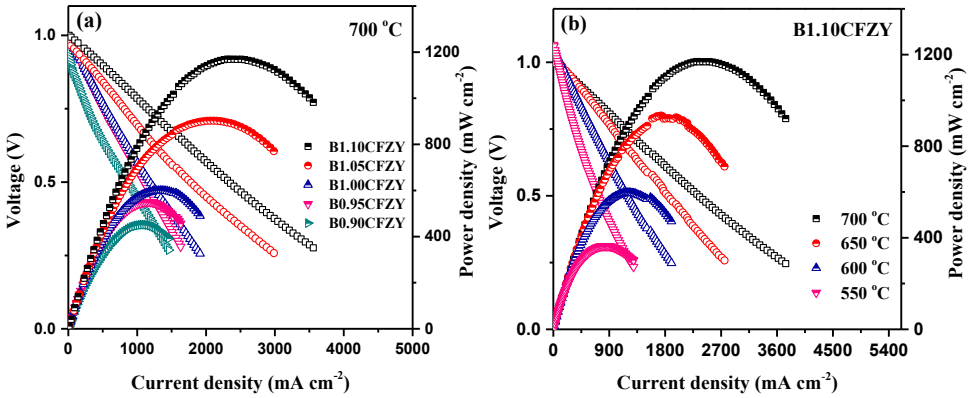

Figure 6. The *I-V* and the corresponding power density of the cells with (a) BxCFZY (x=1.1-0.9) operating at 700°C and (b) B1.1CFZY operating at 700-550°C.

As shown in Figure 7, The resistances of single cells with BxCFZY at 700-550°C were analyzed by EIS. The ohmic resistance (R_o) values of all cells at the same temperature are close, while the polarization resistance (R_p) exhibits a marked increase with decreasing the x value (The Rp values were summarized in Table 2). Singe cell with B1.1CFZY exhibits a very low R_p value of 0.05 Ω cm^2 at 700°C, which includes the Rp from the anode side. For symmetrical cell Ni-BZCY/BZCY/Ni-BZCY, single electrode Rp is measured to be 0.07 Ω cm^2 in 3% H_2O humidified $50H_2/50N_2$ at 700°C[48],

indicating an ultra-low Rp from cathode side for single cell with B1.1CFZY. At the same temperature, it is also smaller than that of other cells with cathodes such as $Ba_{0.9}Co_{0.5}Fe_{0.4}Nb_{0.1}O_{3-\delta}$ [49], $Ba_{0.9}Co_{0.7}Fe_{0.2}Nb_{0.1}O_{3-\delta}$[30], $La_{0.58}Sr_{0.4}Fe_{0.8}Co_{0.2}O_{3-\delta}$ (LSCF)[50] and (La,Sr)MnO_3 (LSM)[51]. On the basis of the Nyquist plots at a medium frequency of 10^3-10^0 Hz, the fast oxygen diffusion and surface exchange kinetics can significantly reduce the polarization resistance. Therefore, the cathodic polarization losses directly reflect the electrocatalytic activity for ORR.[29,32,52] The results indicate that the Ba excess in BxCFZY cathodes exhibited the improved electrocatalytic activity for ORR and thus leaded to a superior electrochemical performance.

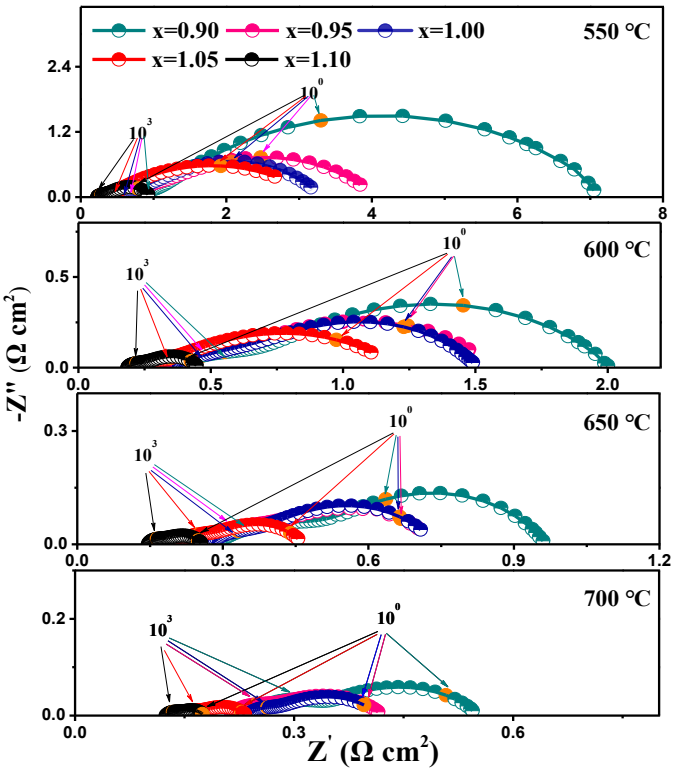

Figure 7. Fitted impedance spectra of the cells with BxCFZY at 700-550°C.

Table 2. Rp Values of Single Cells with BxCFZY (x=1.1-0.9) at 700-550°C.

The cathodic polarization loss usually has an obvious increase when the operating temperature decreases and thus limits the performance of SOFCs. The Rp values of all

cells with BxCFZY cathode significantly increase with decreasing the operating temperature as shown in Figure 8. Remarkably, the Rp of the cell with B1.1CFZY cathode has a slight rise, while those of other BxCFZY (x=0.9-1.05) cathodes increase rapidly as the operation temperature decreases especially at the temperature lower than 600°C. Furthermore, fitted Arrhenius plots shown in Figure S3 demonstrate that the activation energy for ORR reduces from 134.7 to 117.2 kJ mol^{-1} with the barium from deficiency to excess, suggesting that B1.1CFZY with the enhanced ionic diffusion properties exhibits the best catalytical activity for oxygen reduction reaction at reduced temperature. All these results confirmed that the Ba excess in BxCFZY cathodes have a positive effect on cell performance due to the promoted catalytic activity for ORR.

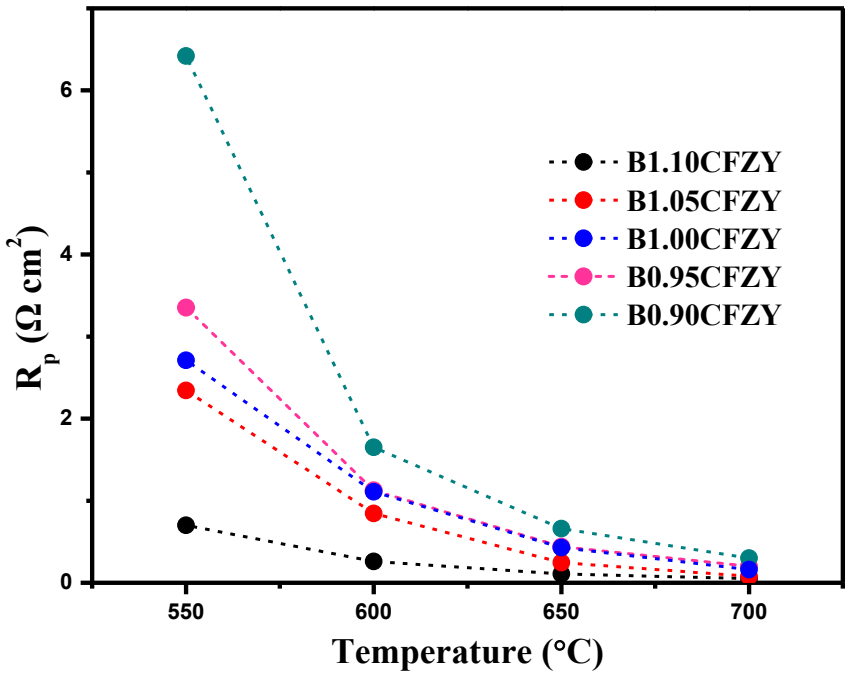

Figure 8. Temperature dependence of the interfacial polarization resistance (R_P) for the cells with BxCFZY (x=1.1-0.9).

3.6. DRT Analysis. To further determine the polarization difference of BxCFZY cathodes, the DRT analysis method was adopted to study the detailed polarization processes of the cells with BxCFZY cathodes as shown in Figure 9. Four separated

peaks exist on the DRT curves which denoted as P1-P4 from high frequency to low frequency, meaning four main rate-determining processes. The contribution rates of different rate-determining processes were summarized in Table 3. The high-frequency peak changes to a lower frequency, usually corresponding to the polarization process from charge transfer, dissociative adsorption or surface exchange of species, to gas diffusion.[29,53-55] It should be noted that the F(τ) peak intensity of P3 and P2 obviously increases with the barium from excess to deficiency. P3 and P2 peaks represent O_2 adsorption/dissociation and oxygen species diffusion at the cathode side, respectively.[29,57] In all BxCFZY samples, P3 peak of Ba1.1CFZY showed the lowest intensity, suggesting the fastest oxygen species involved reactions in Ba1.1CFZY cathode. That's why Ba1.1CFZY cathode exhibited the best catalytic activity for ORR and cell performance.

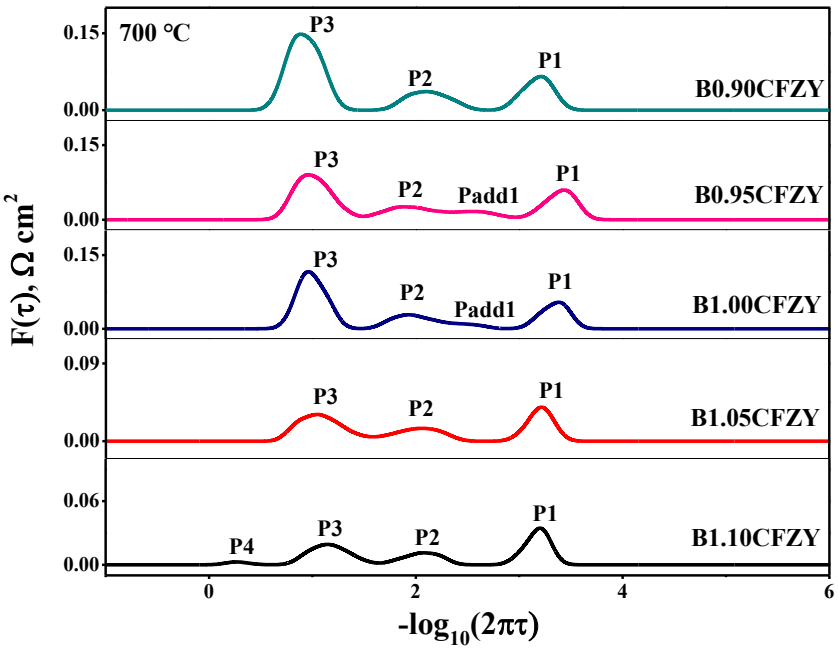

Figure 9. DRT analysis of the impedance spectrum data for the cells with BxCFZY at 700°C.

The P1 intensity of all cells has no obvious change at 700°C, meaning that P1

corresponds to proton formed reactions at the anode side.[58] Padd1 existing between P1 and P2 in Ba1.05CFZY and Ba1.0CFZY may be ascribed to O^{2-} incorporation and transfer in the lattice.[53] Interestingly, P4 peak with the lowest intensity at low frequency appears in Ba1.1CFZY. The formation of P4 may be explained that a large amount of oxygen at the cathode side was transferred to the anodic TPBs, producing a lot of steam that enabled the fuel to be diluted at the anode side. However, the rate-limiting process has a negligible impact on the cell performance due to the low contribution for the entire electrode polarization.

3.7. Characterization of Post-test Cells. The microstructure and elemental distribution of post-test cells were investigated and shown in Figure 10. EDS mapping for the post-test cell with B1.1CFZY shows that the interface between the layers is very clear and uniform. There are no signs of element migration and segregation after test. In addition, the microstructure and specific size of the post-test cells was also measured by SEM as shown in Figure S4. There is no delamination or interfacial reaction for the post-test cells with BxCFZY (x=1.1, 1.0 and 0.95), indicating the excellent chemical compatibility of BxCFZY with electrolyte regardless of the Ba deficiency or excess. The results demonstrate the excellent stability of BxCFZY as the cathode for PCFCs and good chemical compatibility with the electrolyte.

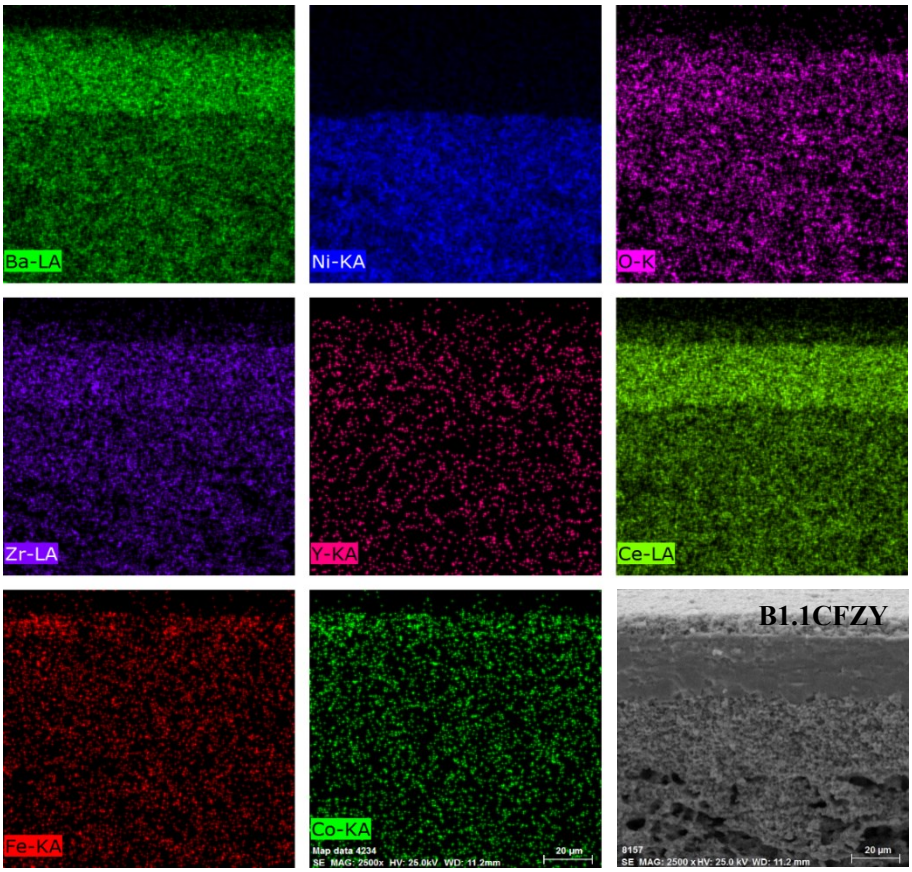

Figure 10. The microstructure and elemental distribution of the post-test cell with B1.1CFZY.

4. CONCLUSIONS

A-site nonstoichiometry of $Ba_xCo_{0.4}Fe_{0.4}Zr_{0.1}Y_{0.1}O_{3-\delta}$ (x=0.9-1.1) was shown to have a significant impact on the crystal structure, oxygen vacancy, electronic conductivity, transfer properties and electrochemical performance. All BxCFZY samples showed cubic symmetrical perovskite structure and the cell parameter increased with the increase in Ba content. Furthermore, the electrical conductivity of BxCFZY perovskite oxides decreased and the oxygen vacancies increased with increasing A-site content. Among the BxCFZY (x=0.9-1.1) series, the cell with B1.1CFZY composition exhibited excellent catalytic activity for ORR and achieved the PPD of 1170 mW cm^{-2} and the Rp of 0.05 Ω cm^2 at 700°C. The DRT analysis confirmed that the B1.1CFZY cathode has the fastest oxygen species involved reactions and diffusion rate. These results

suggested that the A-site excess had a positive effect on BxCFZY as potential cathodes for protonic ceramics fuel cells.

Supporting Information

XRD Rietveld refinement patterns of BxCFZY powders with x=1.1-0.9; EDX image of B1.1CFZY powder used before TEM testing; activation energy (Ea) of the interfacial polarization resistance (R_P) for the cells with BxCFZY (x=1.1, 1.0, 0.9); SEM images of the post-test cells with different cathodes (PDF)

ACKNOWLEDGMENTS

This work was financially supported by the Natural Science Foundation of Jiangxi Province (No. 20224BAB214039), Science and Technology Project of the Education Department of Jiangxi Province (No. GJJ2200867), Doctoral Scientific Research Foundation of Jiangxi University of Science and Technology (No. 205200100639) and U.S. National Science Foundation (1832808).

REFERENCES

(1) Haile, S. M. Fuel Cell Materials and Components. *Acta. Mater.* **2003**, 51, 5981-6000.

(2) Murray, E. P.; Tsai, T.; Barnett, S. A.; A Direct-methane Fuel Cell with a Ceria-based Anode. *Nature* **1999**, 400, 649-651.

(3) Ding, D.; Liu, Z. B.; Li, L.; Xia, C. R. An Octane-fueled Low Temperature Solid Oxide Fuel Cell with Ru-free Anodes. *Electrochem. Commun.* **2008**, 10, 1295-1298.

(4) Adams, T. A; Nease, J.; Tucker, D.; Barton, P. I. Energy Conversion with Solid Oxide Fuel Cell Systems: A Review of Concepts and Outlooks for the Short- and Long-term. *Ind. Eng. Chem. Res.* **2013**, 52, 3089-3111.

(5) Cowin, P. I.; Petit, C. T. G.; Lan, R.; Irvine, J. T. S.; Tao, S. W. Recent Progress in the Development of Anode Materials for Solid Oxide Fuel Cells. *Adv. Energy Mater.* **2011**, 1, 314-332.

(6) Yamazaki, Y.; Hernandez-Sanchez, R.; Haile, S. M. High Total Proton Conductivity in Large-grained Yttrium-doped Barium Zirconate. *Chem. Mater.* **2016**, 21, 2755-2762.

(7) Kreuer, K. D.; Proton-conducting Oxides. *Annu. Rev. Mater. Res.* **2003**, 33, 333-359.

(8) Tong, J. H.; Clark, D.; Hoban, M.; O'Hayre, R. Cost-effective Solid-state Reactive Sintering Method for High Conductivity Proton Conducting Yttrium-doped Barium Zirconium Ceramics. *Solid State Ionics* **2010**, 181, 496-503.

(9) Babilo, P.; Uda, T.; Haile, S. M. Processing of Yttrium-doped Barium Zirconate for High Proton Conductivity. *J. Mater. Res.* **2007**, 22, 1322-1330.

(10) Dusastre, V.; Kilner, J. A. Optimisation of Composite Cathodes for Intermediate Temperature SOFC Applications. *Solid State Ionics* **1999**, 126, 163-174.

(11) He, W.; Dong, F. F.; Wu, X. L.; Ni, M. A highly Active Perovskite Cathode for Low-temperature Solid Oxide Fuel Cells: $BaCo_{0.7}Fe_{0.22}Sc_{0.08}O_{3-\delta}$. *Adv. Sustain. Syst.* **2017**, 1, 1700005.

(12) Duan, C. C.; Hook, D.; Chen, Y. H.; Tong, J. H.; O'Hayre, R. Zr and Y Co-doped Perovskite as a Stable, High Performance Cathode for Solid Oxide Fuel Cells Operating below 500°C. *Energy Environ. Sci.* **2017**, 10, 176-182.

(13) Lee, K. T.; Manthiram, A. Effect of Cation Doping on the Physical Properties and

Electrochemical Performance of $Nd_{0.6}Sr_{0.4}Co_{0.8}M_{0.2}O_{3-\delta}$ (M= Ti, Cr, Mn, Fe, Co, and Cu) Cathodes. *Solid State Ionics* **2007**, 178, 995-1000.

(14) Singh, K.; Sahoo, A.; Thangadurai, V. Oxygen Reduction Reaction Properties of Cobalt-Free Perovskites for SOFCs. *ECS Transactions* **2017**, 78, 479-488.

(15) Zhao, H.; Cheng, Y.; Xu, N.; Li, Y.; Li, F.; Ding, W.; Lu, X. Oxygen Permeability of A-site Nonstoichiometric $BaxCo_{0.7}Fe_{0.2}Nb_{0.1}O_{3-\delta}$ Perovskite Oxides. *Solid State Ionics* **2010**, 181, 354-358.

(16) Yang, C.; Ren, C.; Yu, L.; Jin, C. High Performance Intermediate Temperature Micro-tubular SOFCs with $Ba_{0.9}Co_{0.7}Fe_{0.2}Nb_{0.1}O_{3-\delta}$ as Cathode. *Int. J. hydrogen Energ.* **2013**, 38, 15348-15353.

(17) Wang, H.; Tablet, C.; Feldhoff, A.; Caro, J. Investigation of Phase Structure, Sintering, and Permeability of Perovskite-type $Ba_{0.5}Sr_{0.5}Co_{0.8}Fe_{0.2}O_{3-\delta}$ Membranes. *J. Membr. Sci.* **2005**, 262, 20-26.

(18) Zhao, H.; Shen, W.; Zhu, Z.; Li, X.; Wang, Z. Preparation and Properties of $Ba_xSr_{1-x}Co_yFe_{1-y}O_{3-\delta}$ Cathode Material for Intermediate Temperature Solid Oxide Fuel Cells. *J. Power Sources* **2008**, 182, 503-509.

(19) Harada, M.; Domen, K.; Hara, M.; Tatsumi, T. Oxygen-permeable Membranes of $Ba_{1.0}Co_{0.7}Fe_{0.2}Nb_{0.1}O_{3-\delta}$ for Preparation of Synthesis Gas from Methane by Partial Oxidation. *Chem. Lett.* **2006**, 35, 968-969.

(20) Cheng, Y.; Zhao, H.; Teng, D.; Li, F.; Lu, X.; Ding, W. Investigation of Ba Fully Occupied A-site$BaCo_{0.7}Fe_{0.3-x}Nb_xO_{3-\delta}$Perovskite Stabilized by Low Concentration of Nb for Oxygen Permeation Membrane. *J. Membr. Sci.* **2007**, 322, 484-490.

(21) Duan, C. C.; Tong, J. H.; Shang, M.; Nikodemski, S.; Sanders, M.; Ricote, S.; Almansoori, A.; O'Hayre, R. Readily Processed Protonic Ceramic Fuel Cells with High Performance at Low Temperatures. *Science* **2015**, 349, 1321-1326.

(22) Zhou, C.; Liu, D.; Fei, M.; Wang, X.; Ran, R.; Xu, M.; Wang, W.; Zhou, W.; O'Hayre, R.; Shao, Z. P. Cathode Water Management Towards Improved Performance of Protonic Ceramic Fuel Cells. *J. Power Sources* **2023**, 556, 232403.

(23) Liang, M. Z.; He, Fan.; Zhou, C.; Chen, Y. B.; Ran, R.; Yang, G. M.; Zhou, W.; Shao, Z. P. Nickel-doped $BaCo_{0.4}Fe_{0.4}Zr_{0.1}Y_{0.1}O_{3\text{-delta}}$ as a New High-performance Cathode for Both Oxygen-ion and Proton Conducting Fuel Cells. *Chem. Eng. J.* **2021**, 420, 127717.

(24) Liang, M. Z.; Liu, D. l.; Zhu, Yi. J.; Zhou, W.; Yang, G. M.; Ran, R.; Shao, Z. P. Nickel Doping Manipulation Towards Developing High Performance Cathode for Proton Ceramic Fuel Cells. *J. Electrochem. Soc.* **2022**, 169, 094509.

(25) Wang, X. Y.; Li, W. H.; Zhou, C.; Xu, M. G.; Hu, Z. W.; Pao, C-. W.; Zhou, W.; Shao, Z. P. Enhanced Proton Conduction with Low Oxygen Vacancy Concentration and Favorable Hydration for Protonic Ceramic Fuel Cells Cathode. *ACS Appl. Mater. Interfaces* **2023**, 15, 1339-1347.

(26) Knudsen, J.; Friehling, P. B.; Bonanos, N. Effect of A-site Stoichiometry on Phase Stability and Electrical Conductivity of the Perovskite Las $(Ni_{0.59}Fe_{0.41})O_{3\text{-}\delta}$ and its Compatibility with $(La_{0.85}Sr_{0.15})_{0.91}MnO_{3\text{-}\delta}$ and $Zr_{0.85}Y_{0.15}O_{2.925}$. *Solid State Ionics* **2005**, 176, 1563-1569.

(27) Poulsen, F. W. Defect Chemistry Modelling of Oxygen-stoichiometry, Vacancy

Concentrations, and Conductivity of $(La_{1-x}Sr_x)_yMnO_{3\pm\delta}$. *Solid State Ionics* **2000**, 129, 145-162.

(28) Kostogloudis, G. C.; Ftikos, C. Properties of A-site-deficient $La_{0.6}Sr_{0.4}Co_{0.2}Fe_{0.8}O_{3-\delta}$-Based Perovskite Oxides. Solid State Ionics **1999**, 126, 143-151.

(29) Wei, K.; Li, N.; Wu, Y.; Song, W.; Wang, X.; Guo, L.; Khan, M.; Wang, S.; Zhou, F.; Ling, Y. Characterization and Optimization of Highly Active and Ba-deficient $BaCo_{0.4}Fe_{0.4}Zr_{0.1}Y_{0.1}O_{3-\delta}$-Based Cathode Materials for Protonic Ceramics Fuel Cells. *Ceram. Int.* **2019**, 45, 18583-18591.

(30) Yang, Z. B.; Han, M. F.; Zhu, P.; Zhao, F.; Chen, F. $Ba_{1-x}Co_{0.9-y}Fe_yNb_{0.1}O_{3-\delta}$ (x= 0-0.15, y=0-0.9) as Cathode Materials for Solid Oxide Fuel Cells. *Int. J. hydrogen Energ.* **2011**, 36, 9162-9168.

(31) Liu, Z.; Cheng, L.; Han, M. F. A-site deficient $Ba_{1-x}Co_{0.7}Fe_{0.2}Ni_{0.1}O_{3-\delta}$ Cathode for Intermediate Temperature SOFC. *J. Power Sources* **2011**, 196, 868-871.

(32) Wang, F.; Chen, D.; Shao, Z. Composition and Microstructure Optimization and Operation Stability of Barium Deficient $Ba_{1-x}Co_{0.7}Fe_{0.2}Nb_{0.1}O_{3-\delta}$ Perovskite Oxide Electrodes. *Electrochim. Acta* **2013**, 103, 23-31.

(33) Yang, Y.; Chen, Y.; Tian, D.; Lua, X.; Ding, Y.; Yu, W.; Lin, B. A New A-site Excessive Strategy to Improve Performance of Layered Perovskite Cathode for Intermediate-temperature Solid Oxide Fuel Cells. *Electrochim. Acta* **2017**, 231, 686-693.

(34) Hailstone, R. K.; DiFrancesco, A. G.; Leong, J. G.; Allston, T. D.; Reed, K. J. A Study of Lattice Expansion in CeO_2 Nanoparticles by Transmission Electron Microscopy. *J. Phys. Chem. C* **2009**, 113, 15155-15159.

(35) Kim, Y. M.; He, J.; Biegalski, M. D.; Ambaye, H.; Lauter, V.; Christen, H. M.; Pantelides, S. T.; Pennycook, S. J.; Kalinin, S. V.; Borisevich, A. Y. Probing Oxygen Vacancy Concentration and Homogeneity in Solid-oxide Fuel-cell Cathode Materials on the Subunit-cell Level. *Nat. Mater.* **2012**, 11, 888-894.

(36) He, W.; Wu, X.; Yang, G. M.; Shi, H. G.; Dong, F. F.; Ni, M. $BaCo_{0.7}Fe_{0.22}Y_{0.08}O_{3-\delta}$ as an Active Oxygen Reduction Electrocatalyst for Low Temperature Solid Oxide Fuel Cells below 600°C. *Acs Energy Lett.* **2017**, 2, 301-305.

(37) Stevenson, J. W.; Armstrong, T. R.; Carneim, R. D.; Pederson, L. R.; Weber, W. J. Electrochemical Properties of Mixed Conducting Perovskites $La_{1-x}M_xCo_{1-y}Fe_yO_{3-\delta}$ (M=Sr, Ba, Ca). *J. Electrochem. Soc.* **1996**, 143, 2722.

(38) Chen, Z.; Ran, R.; Zhou, W.; Shao, Z.; Liu, S. Assessment of $Ba_{0.5}Sr_{0.5}Co_{1-y}Fe_yO_{3-\delta}$(y=0.0-1.0) for Prospective Application as Cathode for IT-SOFCs or Oxygen Permeating Membrane. *Electrochim. Acta* **2007**, 52, 7343-7351.

(39) Jaiswal, S. K.; Choi, S. M.; Yoon, K. J.; Son, J. W.; Kim, B. K.; Lee, H. W.; Lee, J. H. Effect of Ba-deficiency on the Phase and Structural Stability of $(BaSr)(CeZr)O_3$-Based Proton Conducting Oxides. *Int. J. Hydrogen Energ.* **2015**, 40, 11022-11031.

(40) Yang, L.; Zuo, C.; Liu, M. High-performance Anode-supported Solid Oxide Fuel Cells Based on $Ba(Zr_{0.1}Ce_{0.7}Y_{0.2})O_{3-\delta}$ (BZCY) Fabricated by A Modified Co-pressing Process. *J. Power Sources* **2010**, 195, 1845-1848.

(41) Nurk, G.; Kooser, K.; Urpelainen, S.; Käämbre, T.; Joost, U.; Kodu, M.; Kivi, I.; Kanarbik, R.; Kukk, E.; Lust, E. Near Ambient Pressure X-ray Photoelectron- and Impedance Spectroscopy Study of $NiO-Ce_{0.9}Gd_{0.1}O_{2-\delta}$ Anode Reduction Using a Novel

Dual-chamber Spectroelectrochemical Cell. *J. Power Sources* **2018**, 378, 589-596.

(42) Jirátová, K.; Mikulová, J.; Klempa, J.; Grygar, T.; Bastl, Z.; Kovanda, F. Modification of Co-Mn-Al Mixed Oxide with Potassium and its Effect on Deep Oxidation of VOC. *Appl. Catal. A: Gen.* **2009**, 361, 106-116.

(43) Song, Y.; Chen, Y.; Wang, W.; Zhou, C.; Zhong, Y.; Yang, G.; Zhou, W.; Liu, M.; Shao, Z. Self-Assembled Triple-conducting Nanocomposite as a Superior Protonic Ceramic Fuel Cell Cathode. *Joule* **2019**, 3, 2842-2853.

(44) Shang, M.; Tong, J. H.; O'Hayre, R. A Promising Cathode for Intermediate Temperature Protonic Ceramic Fuel Cells: $BaCo_{0.4}Fe_{0.4}Zr_{0.2}O_{3-\delta}$. *RSC Adv.* **2013**, 3, 15769-15775.

(45) Hibino, T.; Hashimoto, A.; Suzuki, M.; Sano M. A Solid Oxide Fuel Cell Using Y-doped $BaCeO_3$ with Pd-loaded FeO Anode and $Ba_{0.5}Pr_{0.5}CoO_3$ Cathode at Low Temperatures. *J. Electrochem. Soc.* **2002**, 149, A1503-1508.

(46) Xie, K.; Zhou, J.; Meng, G. Pervoskite-type $BaCo_{0.7}Fe_{0.2}Ta_{0.1}O_{3-\delta}$ Cathode for Proton Conducting IT-SOFC. J. Alloy Comp. **2010**, 506, L8-11.

(47) Wang, W.; Zhang, X.; Zhang, D.; Zeng, Q., Jiang, Y.; Lin, B. Highly Promoted Performance of Triple-conducting Cathode for YSZ-based SOFC Via Fluorine Anion Doping. *Ceram. Int.* **2020**, 46, 23964-23971.

(48) Wang, Q.; Luo, Ting.; Tong, Y.; Dai, M.; Miao, X.- Y.; Ricote, S.; Zhan, Z.; Chen, M. Large-area Protonic Ceramic Cells for Hydrogen Purification. *Sep. Purif. Technol.* **2022**, 295, 121301.

(49) Yang, Z.; Jin, C.; Yang, C.; Han, M.; Chen, F. $Ba_{0.9}Co_{0.5}Fe_{0.4}Nb_{0.1}O_{3-\delta}$ as Novel

Oxygen Electrode for Solid Oxide Electrolysis Cells. *Int. J. Hydrogen Energ.* **2011**, 36, 11572-11577.

(50) Escudero, M. J.; Parada, I. G. D.; Fuerte, A.; Serrano, J. L. Analysis of the Electrochemical Performance of MoNi-CeO_2 Cermet as Anode Material for Solid Oxide Fuel Cell, Part I. H_2, CH_4, and H_2/CH_4 Mixtures as Fuels. *J. Power Sources* **2014**, 253, 64-73.

(51) Leng, Y. J.; Chan, S. H.; Khor, K. A.; Jiang, S. P.; Development of LSM/YSZ Composite Cathode for Anode-supported Solid Oxide Fuel Cells. *J. Appl. Electrochem.* **2004**, 34, 409-415.

(52) He, W.; Yuan, R.; Dong, F.; Wu, X.; Ni, M. High Performance of Protonic Solid Oxide Fuel Cell with $BaCo_{0.7}Fe_{0.22}Sc_{0.08}O_{3-\delta}$ Electrode. *Int. J. Hydrogen Energ.* **2017**, 42, 25021-25025.

(53) Shi, N.; Su, F.; Huan, D. M.; Xie, Y.; Lin, J.; Tan, W. Z.; Peng, R. R.; Xia, C. R.; Chen, C. S.; Lu, Y. L. Performance and DRT Analysis of P-SOFCs Fabricated Using New Phase Inversion Combined Tape Casting Technology. *J. Mater. Chem.* **2017**, 5, 19664-19671.

(54) Wang, A.; Wang, X.; Qiu, P.; Yang, J. J.; Yang, X. F.; Hua, S. Y.; Chi, Bo.; Pu, J.; Li. J. Performance and Durability of an Anode-supported Solid Oxide Fuel Cell with a PdO/ZrO_2Engineered $(La_{0.8}Sr_{0.2})_{0.95}MnO_{3-\delta}$-$(Y_2O_3)_{0.08}(ZrO_2)_{0.92}$ Composite Cathode. *Int. J. Hydrogen Energ.* **2018**, 43, 12368-12376.

(55) Sikstrom, D.; Javed, A.; Muhammad, S.; Thangadurai, V. Perovskite-type $Nd_{0.75}Ba_{0.25}Co_{0.8}Fe_{0.2}O_{3-\delta}$ Cathode for Intermediate Temperature Solid Oxide Fuel Cells.

Ionics **2023**, 29, 1507-1514.

(56) Oz, A.; Singh, K.; Gelman, D.; Thangadurai, V.; Tsur, Y. Understanding of Oxygen Reduction Reaction on Perovskite-Type $Ba_{0.5}Sr_{0.5}Fe_{0.91}Al_{0.09}O_{3-\delta}$ and $Ba_{0.5}Sr_{0.5}Fe_{0.8}Cu_{0.2}O_{3-\delta}$ Using AC Impedance Spectrosc. *J. Phys. Chem. C* **2018**, 122, 15097-15107.

(57) Liu, B.; Muroyama, H.; Matsui, T.; Tomida, K.; Kabata, T.; Eguchi, K. Analysis of Impedance Spectra for Segmented-in-series Tubular Solid Oxide Fuel Cells. *J. Electrochem. Soc.* **2010**, 157, B1858-1864.

(58) Barfod, R.; Mogensen, M.; Klemenso, T.; Hagen, A.; Liu, Y. L.; Vang, H. P. Detailed Characterization of Anode-supported SOFCs by Impedance Spectroscopy. *J. Electrochem. Soc.* **2007**, 154, B371-378.